High-pressure neutron-diffraction study of the metallization process in $PrNiO_3$

M. Medarde and J. Mesot
Laboratory for Neutron Scattering, ETH&PSI, 5232 Villigen PSI, Switzerland

P. Lacorre
Laboratoire des Fluorures, Université du Maine, Avenue Olivier-Messiaen, 72017 LeMans CEDEX, France

S. Rosenkranz and P. Fischer
Laboratory for Neutron Scattering, ETH&PSI, 5232 Villigen PSI, Switzerland

K. Gobrecht
Institut Laue Langevin, Boîte Postale 156, 38042 Grenoble Cedex 9, France
(Received 17 April 1995; revised manuscript received 7 June 1995)

The modifications of the crystallographic and magnetic structures of $PrNiO_3$ associated with the decrease of the metal-insulator transition temperature, T_{MI}, with external pressure ($P_{ext} \approx 5$ kbar) have been investigated by means of neutron powder diffraction. Our results indicate that the symmetry of the unit cell (orthorhombic *Pbnm* at ambient pressure), is preserved in the pressure range studied. The changes observed in the Ni-O distance and the Ni-O-Ni superexchange angle are, however, similar in sign but very different in magnitude from those obtained by applying an equivalent "internal" pressure. The antiferromagnetic ordering observed at ambient pressure for $T < T_{MI}$ remains unchanged for $P_{ext} < 5$ kbar. This finding is in strong contrast with the results of high-pressure electrical resistance measurements, where a reentrant metallic behavior was observed for $P > 4$ kbar and $T < 65$ K.

I. INTRODUCTION

$RNiO_3$ perovskites (R = rare earth) provide a remarkable opportunity to study the relationship between structural and physical properties, since, by moving along the $4f$ rare-earth series, the evolution of several transport and magnetic properties can be nicely correlated with steric effects associated with the lanthanide contraction. The best example is given by the metal-insulator (MI) transition discovered for the compounds with $R \neq La$,[1] whose transition temperature T_{MI} decreases when the size of the rare-earth ion increases. This decrease is controlled by the tilting angle ω of the NiO_6 octahedra (see the Appendix), whose cosine is, to a first approximation, a linear function of T_{MI}.[2]

The MI temperature can also be lowered by applying an external pressure P_{ext}. The pressure dependences of T_{MI} reported by Canfield *et al.*[3] and by Obradors *et al.*[4] are displayed in Fig. 1. Although in both papers $\partial T_{MI}/\partial P_{ext}$ is negative, it is surprising to note that their results are only coincident in the low-pressure range ($P < 5$ kbar). In spite of this discrepancy, which may be due to differences in the method of determining T_{MI}, two important facts can be retained from the former data. First, T_{MI} is extraordinarily sensitive to pressure. The values of $\partial T_{MI}/\partial P_{ext}$ given by Obradors *et al.*[4] and by Canfield *et al.*[3] are -4.2 K/kbar and -7.6 K/kbar, respectively, (note that the last value is a linear average over the studied pressure range). To our knowledge, the only other oxides that show comparable pressure coefficients are the $V_N O_{2N-1}$ Magneli series, whose values of $\partial T_{MI}/\partial P_{ext}$ for $N = 2$, 6, 8, and ∞ are displayed in Table I.

Second, in both publications the data corresponding to all the nickelates studied can be superimposed to form a universal curve (see the caption of Fig. 1). This behavior strongly suggests that a common structural and/or electronic parameter is controlling the variation of the T_{MI} under pressure. By extrapolating the behavior observed in the case of an *internal* pressure (substitution of the rare-earth ion by another with a larger ionic radius), both Canfield *et al.* and Obradors *et al.* associated the de-

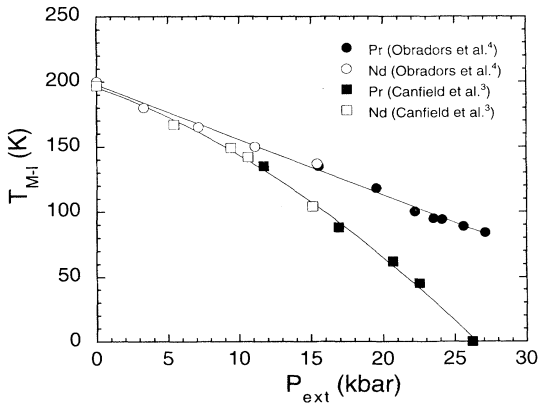

FIG. 1. Pressure dependence of T_{MI} for $NdNiO_3$ (open symbols, unshifted) and $PrNiO_3$ (full symbols, shifted by +15.5 kbar). The circles are data from Ref. 4 and the squares from Ref. 3.

TABLE I. MI transition temperatures at ambient pressure, investigated pressure ranges and $\partial T_{MI}/\partial P_{ext}$ coefficients for some oxides and sulfides showing MI transitions as a function of temperature. (*) Linear dependence of T_{MI} with P_{ext}. (○) Nonlinear dependence of T_{MI} with P_{ext}. In this last case, $\partial T_{MI}/\partial P_{ext} = \Delta T_{MI}/\Delta P_{ext}$ in the pressure range studied.

Compound	T_{MI} (K)	P_{max} (kbar)	$\partial T_{MI}/\partial P_{ext}$ (K/kbar)
V_2O_3($N=2$) (Ref. 26)	170	24	−7.08 (○)
V_6O_{11}($N=6$) (Ref. 27)	157	20	−1.60 (*)
V_8O_{15}($N=8$) (Ref. 27)	67	14	−4.78 (○)
$V_{0.98}Cr_{0.02}O_{15}$ (Ref. 27)	115	20	−1.75 (*)
VO_2($N=\infty$) (Ref. 28)	68	40	+1.082 (*)
NiS (Ref. 29)	210	20	−10.50 (○)

crease of T_{MI} with the variation of the tilting angle, ω, of the NiO_6 octahedra. However, their conclusions are controversial since *they predict, respectively, a negative and a positive sign for* $\partial\omega/\partial P_{ext}$. The experimental determination of this sign was one of the objectives of this work.

The second objective concerns the dependence of the magnetic structure with pressure. As it is also shown in Refs. 3 and 4, a reentrant metallic behavior is observed for lower temperatures and higher pressures than a R-dependent critical point (T_{cr},P_{cr}) (i.e., $T_{cr} \approx 65$ K and $P_{cr} \approx 4$ kbar for $PrNiO_3$). This behavior has been explained as follows:[4] below T_{MI}, the metallic phase transforms progressively into the insulating phase. Due to the application of high pressures, the transformation rate decreases, being finally inverted below T_{cr}. Then the metallic phase, more stable under pressure, again becomes dominant, and the reentrant metallic behavior is observed. Although this interpretation is consistent with the hysteresis of the electrical resistance observed at ambient pressure below T_{MI},[5] several questions remain: What is the nature of the metallic phase observed at low temperature? Is it magnetic? And, in this case, how are the localized Ni magnetic moments of the low-temperature insulating phase affected when the system again becomes metallic below T_{cr}?

In order to answer these questions, we have performed several neutron-diffraction experiments at high hydrostatic pressure (4.7 kbar) and different temperatures (from 5 K to RT) on a $PrNiO_3$ powder sample. In Sec. IV, the evolution of the crystallographic structure between ambient pressure and 4.7 kbar is analyzed and compared with results obtained by applying an equivalent internal pressure. The implications of these results on the anomalously high-pressure coefficient of $RNiO_3$ perovskites are also briefly discussed. In Sec. V, the magnetic nature of the low-temperature phase ($T < T_{cr}$) is clearly established and discussed by comparing the experimental conditions of the neutron diffraction and electrical resistance measurements.

II. EXPERIMENT AND DATA ANALYSIS

The synthesis of the polycrystalline sample used in this work has been described elsewhere.[1] Previous x-ray and neutron-diffraction experiments at ambient pressures showed the material to be well crystallized and virtually free of structural defects. The only observed impurity was a small amount of NiO (2% of the total weight).

High-pressure experiments on powder diffractometers equipped with multidetectors are extremely difficult to realize since, with conventional materials like steel or aluminum, the diffraction data contain Bragg scattering from the cell itself. These unwanted reflections can be orders of magnitude larger than the reflections from the sample, thus rendering impossible a precise structure refinement. In order to avoid these problems, we have developed a zero-matrix pressure cell whose walls are made of an alloy of Ti and Zr. Since these two elements have coherent scattering lengths (CSL) of opposite sign, it is possible to prepare a material whose averaged CSL is equal to zero. No Bragg reflections from the pressure cell will then contribute to the diffraction pattern. The inner and outer diameters of the cell at the sample position are 1 and 2 cm, respectively, and the height of the neutron-illuminated part of the cell is 5 cm. In order to have perfectly hydrostatic conditions we used helium gas as a transmitting medium. The pressure P_{ext} can be changed *in situ* in the $0 \leq P_{ext} \leq 5$ kbar range. The cell is mounted into a helium cryostat and temperatures as low as 2 K can be reached. Below a critical temperature (e.g., 50 K at 5 kbar) helium crystallizes and contributes to the diffraction pattern. Through the determination of the helium unit-cell volume one can calibrate the pressure even at the lowest temperatures.

The experiments were performed in the Saphir reactor at the Paul Scherrer Institut (Würenlingen). In this work, the DMC diffractometer[6] operating in both high resolution (HR) ($\lambda = 1.6959$ Å, $\alpha_1 = 10'$, $\alpha_2 = \infty$, $\alpha_3 = 15'$, 2θ step $= 0.1°$) and high intensity (HI) modes ($\lambda = 1.7000$ Å, $\alpha_1 = 40'$, $\alpha_2 = \infty$, $\alpha_3 = 15'$, 2θ step $= 0.2°$) was used. Several neutron powder-diffraction patterns were recorded at ≈ 4.7 kbar at the following temperatures: 300, 135, 95, and 5 K, the first two in HR mode and the last two in both HR and HI modes. An additional room temperature (RT) ambient-pressure HR diffraction pattern was also taken to calibrate the wavelength. The scattering coming from the cryostat and the pressure cell was minimized by using an oscillating radial collimator.[6]

The Rietveld method was used to refine both the crystallographic and the magnetic structures. All the data were analyzed with the program FULLPROF,[7] which allows the simultaneous treatment of several crystallographic and magnetic phases. In order to diminish the number of free parameters, the background was described by interpolating between several selected points. The pseudo-Voigt function and the usual Caglioti, Paoletti, and Ricci[8] formula were used to describe the profile and the full width at half maximum of the Bragg reflections.

Due to the smallness of the expected structural changes, special case was taken to analyze the data in a consistent way. The wavelength was corrected and the zero point of the diffractometer established by fitting the RT ambient-pressure HR pattern with previously published structural data obtained in the same conditions.[9]

Further refinement of the profile parameters indicated that U, V, W, and the mixing parameter of the pseudo-Voigt function η were very close to the nominal values for the resolution function of the instrument. They were then fixed in the refinement of the remaining HR patterns, the only free parameters being the lattice parameters (3), the atomic coordinates (7), the isotropic temperature factors (3), the scale factor, and the lattice parameter of NiO (1). The number of independent reflections in the accessible half-reciprocal space ($2\theta_{max}=134.8$) was 161.

For the HI patterns, the structural parameters were fixed to those obtained in the HR refinement at the same temperature. The only free parameters were then U, V, W, η, the scale factor and, for the low-temperature measurements, the magnetic moment of Ni and the lattice parameters of solid hcp He(2). The number of accessible reflections ($2\theta_{max}=88.8$) was in this case 147 (71 nuclear and 76 magnetic).

III. RESULTS

Figure 2(a) shows the RT neutron-diffraction pattern of $PrNiO_3$ measured on the DMC diffractometer at ambient pressure in a standard vanadium container using the HI mode. In Figures 2(b) and 2(c), the same pattern recorded at 4.7 kbar and lower temperatures (95 and 5 K, respectively) is displayed, the most striking difference being the increase of the incoherent background due to the pressure cell. Note, however, that it is very flat, with any extra peak coming from the sample environment. The peak-to-background ratio is approximately 5:1, and no preferential orientations and/or distortions in the peak shape can be observed. This is in strong contrast with most of the actually available high-pressure neutron-diffraction data, where the former problems usually make a careful, high-quality, structural analysis very difficult. By using the HR mode, a substantial improvement of the peak-to-background ratio was reached (roughly from 5:1 to 7:1). It is illustrated in Fig. 2(d), which shows the neutron-diffraction pattern recorded at RT and 4.7 kbar.

By looking at the low angle part of Figs. 2(a) and 2(b), the appearance of new, very small peaks, indexables with a propagation vector $\mathbf{k}=(1/2\,0\,1/2)$ is observed (see inset). The origin of these reflections, whose existence is more clearly shown in Fig. 2(c), will be addressed later in the discussion. The peaks marked with an asterisk are the (100) and (101) reflections of solid He, which, at 4.7 kbar, solidifies at ≈ 37 K in a hcp hexagonal phase. Due to strong preferential orientation, only these two peaks are clearly visible.

IV. STRUCTURAL STUDY

A. $PrNiO_3$ at 4.7 kbar

The crystallographic structure of $PrNiO_3$ at 4.7 kbar and RT was first refined by using the same *Pbnm* space group adopted by this compound at ambient pressure.[9] In Fig. 3, we see that the agreement between the observed and calculated patterns is very good. The same situation was found at lower temperatures, indicating that the stability of the structure is preserved in the range of pres-

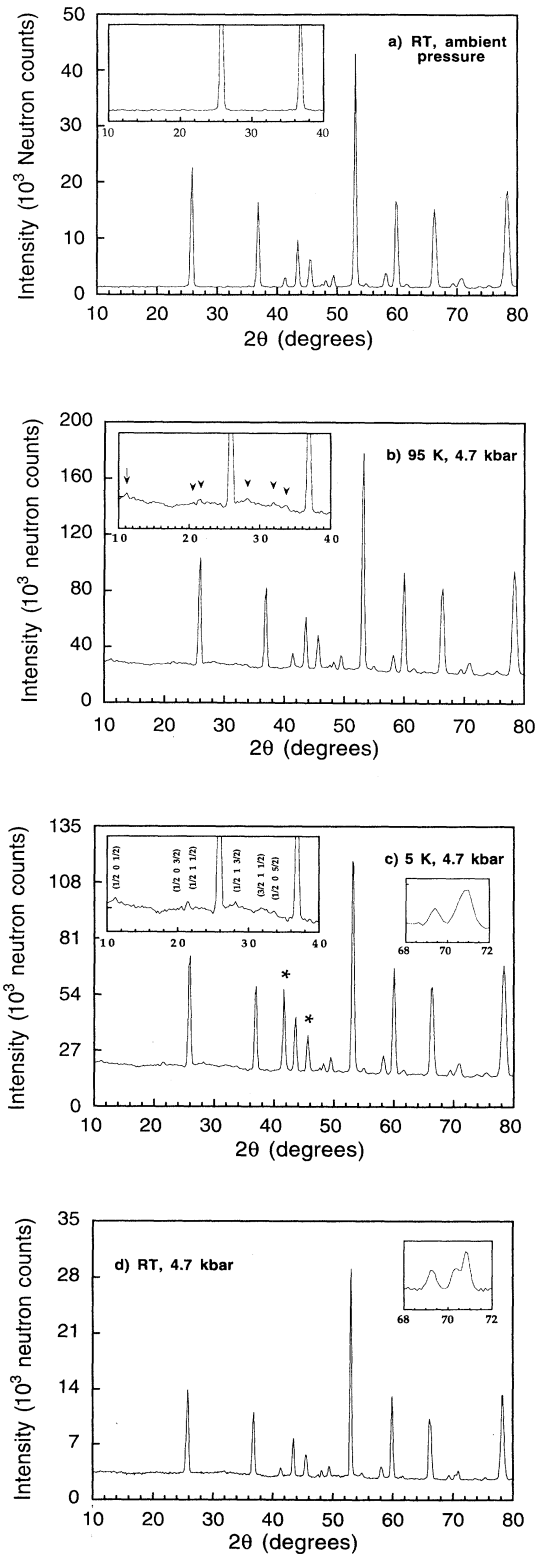

FIG. 2. Neutron powder-diffraction pattern of $PrNiO_3$ recorded using the high intensity mode. (a) In a vanadium can at room temperature and ambient pressure. (b) In the zero-matrix high-pressure cell at 4.7 kbar and 95 K. (c) In the same conditions at 5 K. In (d) a high-resolution pattern recorded at 4.7 kbar and RT is displayed.

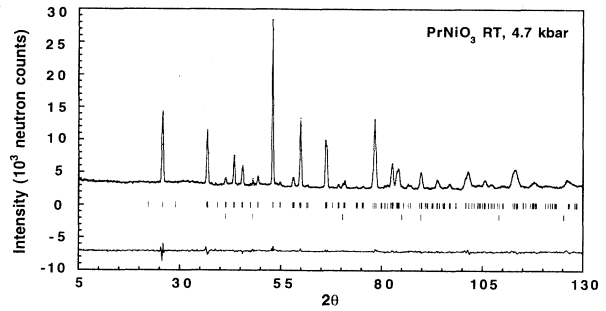

FIG. 3. Neutron-diffraction pattern of $PrNiO_3$ recorded at RT and 4.7 kbar in HR mode. Points represent the raw data. The solid line is the calculated profile. The vertical marks show the position of allowed reflections. The first row correspond to the nuclear reflections of $PrNiO_3$ and the second row to those of NiO.

sures studied. The refined structural parameters at RT, 135, 95, and 5 K are listed in Table II, together with the reliability factors. Some relevant interatomic distances and angles are also displayed in Table III.

The variations of the lattice parameters and the unit-cell volume with pressure are shown in Fig. 4. Their values at 4.7 kbar (full dots) are systematically smaller

TABLE II. Structural and lattice parameters for $PrNiO_3$ at 4.7 kbar.

$PrNiO_3$				
Temperature	RT	135 K	95 K	5 K
Pressure	4.7 kbar	4.7 kbar	4.7 kbar	4.7 kbar
Space group	*Pbnm*	*Pbnm*	*Pbnm*	*Pbnm*
Pr(4*c*)				
(*x y* 1/4)				
x	0.995(2)	0.997(2)	0.994(1)	0.993(1)
y	0.024(1)	0.033(1)	0.034(1)	0.032(1)
B (Å^2)	1.01(7)	0.1(1)	0.16(7)	0.13(7)
Ni(4*b*)				
(1/2 0 0)				
B (Å^2)	0.73(3)	0.08(5)	0.09(4)	0.07(3)
O(1)(4*c*)				
(*x y* 1/4)				
x	0.0656(9)	0.068(1)	0.0707(9)	0.0711(8)
y	0.495(1)	0.492(2)	0.493(1)	0.492(1)
B (Å^2)	0.8(1)	0.26(5)	0.23(4)	0.21(3)
O(2)(8*d*)				
(*x y z*)				
x	0.7197(5)	0.7181(7)	0.7181(5)	0.7184(5)
y	0.2786(5)	0.2797(7)	0.2823(5)	0.2812(5)
z	0.0346(4)	0.0348(6)	0.0361(4)	0.0369(4)
B (Å^2)	1.18(7)	0.26(5)	0.23(4)	0.21(3)
a (Å)	5.4152(2)	5.4074(2)	5.4092(2)	5.4124(1)
b (Å)	5.3732(2)	5.3705(3)	5.3765(2)	5.3805(2)
c (Å)	7.6185(3)	7.6083(4)	7.6138(3)	7.6122(2)
Ni moment (μ_B)			0.86(7)	0.92(6)
R_{wp} (%)	2.86	4.25	2.84	2.83
R_{exp} (%)	1.67	2.25	1.77	1.94
χ^2	2.94	3.56	2.56	2.14
R_B (%)	6.10	4.52	3.36	3.05
R_{mag} (%)			37.5	32.3

TABLE III. Selected distances and angles for $PrNiO_3$ at 4.7 kbar calculated from the parameters shown in Table I.

$PrNiO_3$				
Temperature	RT	135 K	95 K	5 K
Pressure	4.7 kbar	4.7 kbar	4.7 kbar	4.7 kbar
Space group	*Pbnm*	*Pbnm*	*Pbnm*	*Pbnm*
$d_{Ni\text{-}O(1)}$ (×2)	1.938(1)	1.938(1)	1.942(1)	1.942(1)
$d_{Ni\text{-}O(2)}$ (×2)	1.930(3)	1.928(4)	1.942(3)	1.940(3)
(×2)	1.946(3)	1.948(4)	1.942(3)	1.946(3)
$\langle d_{Ni\text{-}O} \rangle$	1.938(1)	1.938(1)	1.942(1)	1.943(1)
Ni-O(1)-Ni (×2)	158.8(2)	157.9(3)	157.2(2)	157.0(2)
Ni-O(2)-Ni (×4)	159.4(5)	158.9(7)	158.1(5)	158.1(5)
⟨Ni-O-Ni⟩	159.2(2)	158.6(3)	157.8(2)	157.7(2)
$\langle \omega \rangle$	10.4(1)	10.7(1)	11.1(1)	11.2(1)
$d_{Pr\text{-}O(1)}$	2.38(1)	2.36(1)	2.365(9)	2.371(8)
$d_{Pr\text{-}O(1)}$	3.04(1)	3.06(1)	3.062(9)	3.059(8)
$d_{Pr\text{-}O(1)}$	2.87(1)	2.93(1)	2.934(8)	2.937(8)
$d_{Pr\text{-}O(1)}$	2.56(1)	2.49(1)	2.506(8)	2.510(8)
$d_{Pr\text{-}O(2)}$ (×2)	2.406(6)	2.424(8)	2.408(6)	2.400(5)
$d_{Pr\text{-}O(2)}$ (×2)	2.606(7)	2.590(9)	2.582(6)	2.575(6)
$d_{Pr\text{-}O(2)}$ (×2)	3.119(6)	3.145(8)	3.171(6)	3.171(5)
$d_{Pr\text{-}O(2)}$ (×2)	2.702(6)	2.673(7)	2.682(5)	2.696(5)
$\langle d_{Pr\text{-}O} \rangle$	2.710(2)	2.710(3)	2.713(2)	2.714(1)

than at ambient pressure (open dots). The arrows in the figure indicate the metal-insulator temperatures at ambient pressure ($T_{MI}=130$ K) and 4.7 kbar ($T_{MI}=100$ K from Canfield *et al.*,[3] 110 K from Obradors *et al.*,[4] 105 K in average).

The pressure dependence of the average Ni-O distance $d_{Ni\text{-}O}$ and the average tilting angle ω are summarized in Table III and illustrated in Fig. 5. As expected, their variations are rather small. However, it is clear that all of them decrease by applying pressure. The sign of $\partial\omega/\partial P_{ext}$ is then *negative* as predicted by Canfield *et al.*[3]

Several conclusions can be inferred from this result. The first is that, in contrast with previous predictions,[3] the pressure-induced structural changes in the perovskite compounds with the $GdFeO_3$-type perovskite structure (*Pbnm* space group) are not universal. While in $RNiO_3$ and probably $RFeO_3$ (R = La, Pr, Gd, and Tm) (Ref. 10) a less distorted structure with smaller tilting angles is stabilized at high pressures, in $NaMnO_3$ (Ref. 11) and in the $Fe_{1-x}Mg_xSiO_3$ series[12] both ω and the distortion of the perovskite structure increase with pressure.

This different behavior of the *Pbnm*-ABX_3 compounds can be easily understood by comparing the compressibilities κ_L and κ_l of the A-X and B-X bonds. These two quantities are related with $[\partial(\cos\omega_1)/\partial P_{ext}]_T$ and $[\partial(\cos\omega_2)/\partial P_{ext}]_T$ via

$$\left[\frac{\partial\cos\omega_1}{\partial P_{ext}}\right]_T=\frac{x}{2}\left[\cos\omega_1-\frac{1}{3}\cos^3\omega_1\right](\kappa_l-\kappa_L)\,, \quad (1)$$

$$\left[\frac{\partial\cos\omega_2}{\partial P_{ext}}\right]_T=\frac{x}{2}\left[\cos\omega_2-\frac{1}{3\cos\omega_2}\right](\kappa_l-\kappa_L) \quad (2)$$

with $x\approx 1$ (see the appendix for the definition of x, ω_1, ω_2, κ_L, κ_l and for the details of the calculation).

Since the trigonometric factors in expressions (1) and (2) are positive for reasonable values of ω_1 and ω_2 ($\omega_1 < 90°, \omega_2 < 54.7°$) the sign of the derivatives is determined by $(\kappa_l - \kappa_L)$.

In the case of $PrNiO_3$, only $\kappa_l = \kappa_{Ni\text{-}O}$ can be calculated from our neutron-diffraction data (see Table IV). The reason is that, in formula (1), κ_L is the compressibility of the A-X bond when A is in *octahedral* coordination (see the Appendix). In $PrNiO_3$, Pr is not in coordination 6 but 12 (or 8, if we neglect the 4 more distant O nearest neighbors). From the discussion of Hazen and Prewitt,[13] bonds with cations of high coordination or small valence expand or compress more rapidly than those with cations of low coordination or large valence. In the case of L ($Pr^{+3}-O^{-2}$) and l ($Ni^{+3}-O^{-2}$) both the valence (+3) and the coordination (6) of the two cations are exactly the same, and, in consequence, it is not possible to predict which of the two bonds will display the larger compressibility. However, as for $PrNiO_3$ ω decreases with pressure, we should admit that $\kappa_l > \kappa_L$.

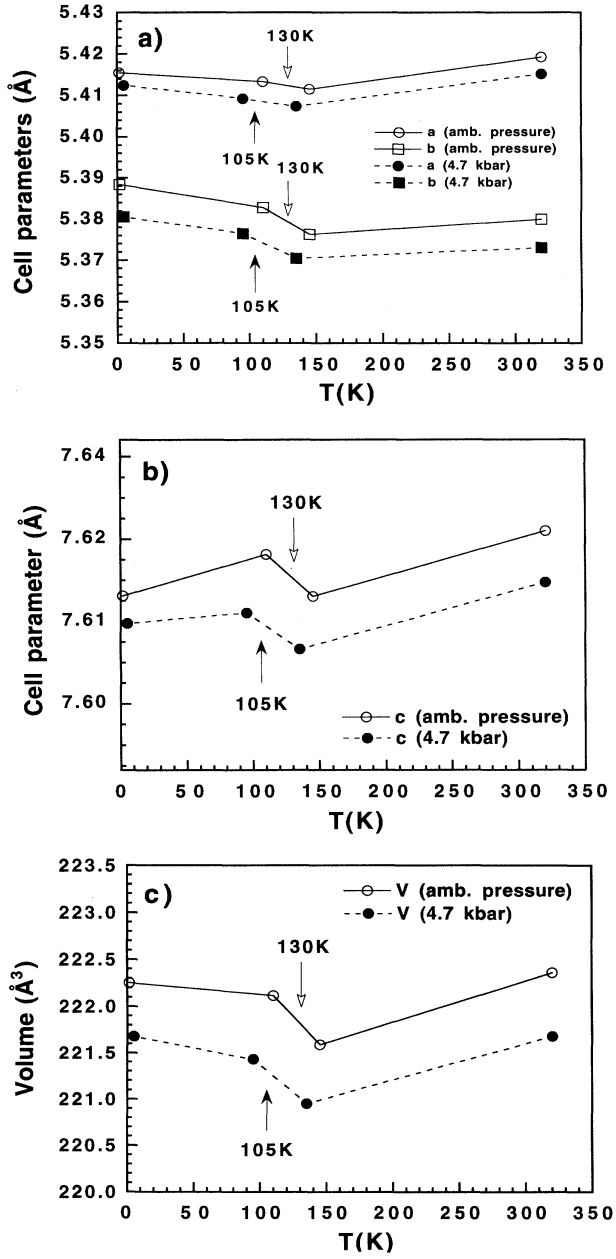

FIG. 4. Pressure dependence of the lattice parameters and the unit-cell volume of $PrNiO_3$ at different temperatures. The error bars are in all the cases smaller than the size of the points. The dotted lines are guides for the eye.

The observed variations of ω and $d_{Ni\text{-}O}$ also allow a simple interpretation of the unusually high value of dT_{MI}/dP_{ext} reported for the nickelates. Taking into account that they belong to the family of charge-transfer insulators (low Δ metals above T_{MI}),[14] we can write the band gap in the insulating phases as $E_g = \Delta - W$. Here, Δ is the charge-transfer energy and W is the O $2p$-like bandwidth, which, to a first approximation, can be written as[15]

$$W \approx \frac{\cos\omega}{d_{Ni\text{-}O}^{3.5}} . \quad (3)$$

As Δ is practically invariant along the series,[2] the metallization of the system under pressure is controlled by the increase of W. From our experience, both ω and $d_{Ni\text{-}O}$ decrease by applying an external pressure. Thus, both contribute to the increase of W. A quick decrease of T_{MI} is then expected. If, as in $Fe_{1-x}Mg_xSiO_3$ and $NaMnF_3$, $d\omega/dP_{ext}$ were positive, the stabilization of the metallic state would be due only to the decrease of the Ni-O distance, which would override the narrowing of W produced by the increase of the tilt angle. The broadening of W would probably be smaller and the decrease of T_{MI} slower.

B. Comparison between the effects of the "internal" and "external" pressures

As was pointed out in the introduction, both mechanisms result in a decrease of the MI transition temperature. However, nothing was known up to now about the differences between the structural modifications produced by external and internal pressures. For this purpose we have compared the data obtained for $PrNiO_3$ at 4.7 kbar ($T_{MI} \approx 105$ K) with those of another nickelate having a similar MI temperature at ambient pressure. The selected compound has been the solid solution $La_{0.3}Nd_{0.7}NiO_3$, whose effective ionic radius r is

$$r(La_{0.3}Nd_{0.7}) = 0.3 \times r(La) + 0.7 \times r(Nd) = 1.124 \text{ Å} , \quad (4)$$

which is slightly bigger than that of Pr($r = 1.126$ Å),[16] and whose MI temperature ($T_{MI} \approx 104$ K) is very close to that expected for $PrNiO_3$ at 4.7 kbar (≈ 105 K).[17]

Figure 6 shows the thermal behavior of d_{NiO} and ω for $PrNiO_3$ and $La_{0.3}Nd_{0.7}NiO_3$ at ambient pressure. By increasing the effective radius o the rare earth, $d_{Ni\text{-}O}$ remains practically unchanged. However, a decrease of the tilt angle is observed. This contrasts with the external pressure results [see Figs. 5(a) and 5(b)], where the difference between the variations of $d_{Ni\text{-}O}$ and ω is less pronounced. The structural modifications responsible for

TABLE IV. Compressibilities κ of the cell parameters, cell volume, $d_{\text{Ni-O}}$, $d_{R\text{-O}}$, and ω. At each temperature, κ has been calculated as $\kappa=-[\alpha(P_f)-\alpha(P_i)]/[P_f-P_i]\alpha(P_i)$ with $P_f=4.7$ kbar, $P_i=0$ kbar, and α one of the crystallographic parameters.

$PrNiO_3$ Temperature	5–1.5 K	95–110 K	135–145 K	RT
a	1.22×10^{-4}	1.61×10^{-4}	1.61×10^{-4}	1.61×10^{-4}
b	3.12×10^{-4}	2.49×10^{-4}	2.30×10^{-4}	2.73×10^{-4}
c	1.17×10^{-4}	2.48×10^{-4}	2.23×10^{-4}	2.18×10^{-4}
V	5.51×10^{-4}	6.56×10^{-4}	6.14×10^{-4}	6.51×10^{-4}
$\langle$Ni-O-Ni$\rangle$	-1.35×10^{-4}	-1.35×10^{-4}	-4.03×10^{-4}	-6.70×10^{-4}
$\langle d_{\text{Ni-O}}\rangle$	1.09×10^{-4}	2.19×10^{-4}	2.19×10^{-4}	4.38×10^{-4}
$\langle d_{\text{Pr-O}}\rangle$	1.57×10^{-4}	1.57×10^{-4}	1.57×10^{-4}	3.14×10^{-4}

the T_{MI} decrease are then not exactly the same under external and internal pressures. In the first case, both d_{NiO} and ω contribute to the stabilization of the metallic state. In the second case, the contribution of ω is dominant, $d_{\text{Ni-O}}$ remaining practically constant. This result has to be considered in any further calculation of the electronic structure of these compounds.

The relative variation of the different crystallographic observables α as a function of the T_{MI} decrease can be evaluated using the parameter $\zeta(\alpha)$, defined as

$$\zeta(\alpha)=\frac{\partial\alpha}{\partial T_{\text{MI}}}\frac{1}{\alpha(P_{\text{ext}}=0)} . \tag{5}$$

The results obtained for d_{NiO} and θ ($\theta=\pi-2\omega$) are

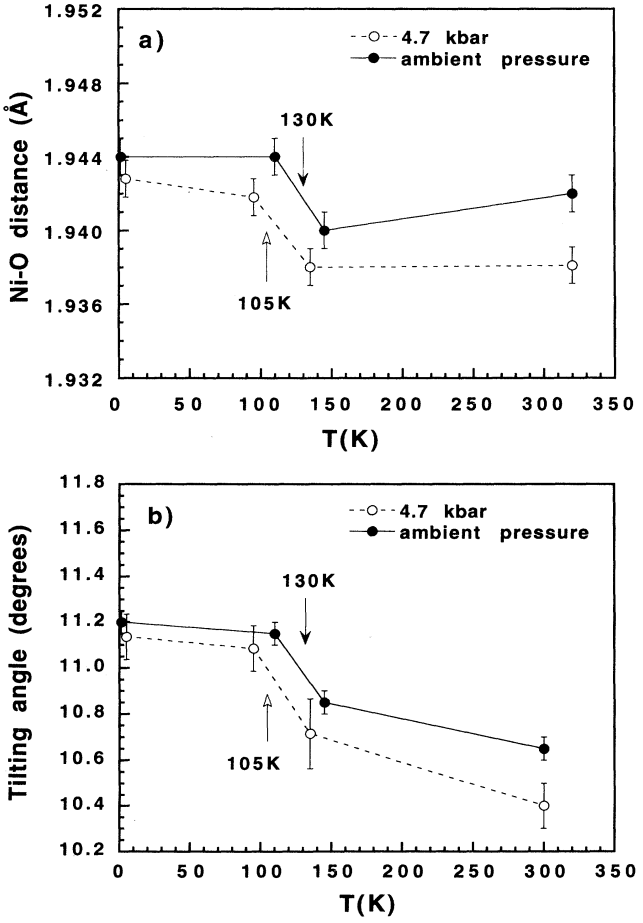

FIG. 5. Pressure dependence of the average Ni-O distance $d_{\text{Ni-O}}$ and the average tilting angle of the NiO_6 octahedra ω for $PrNiO_3$ at different temperatures. The dotted lines are guides for the eye.

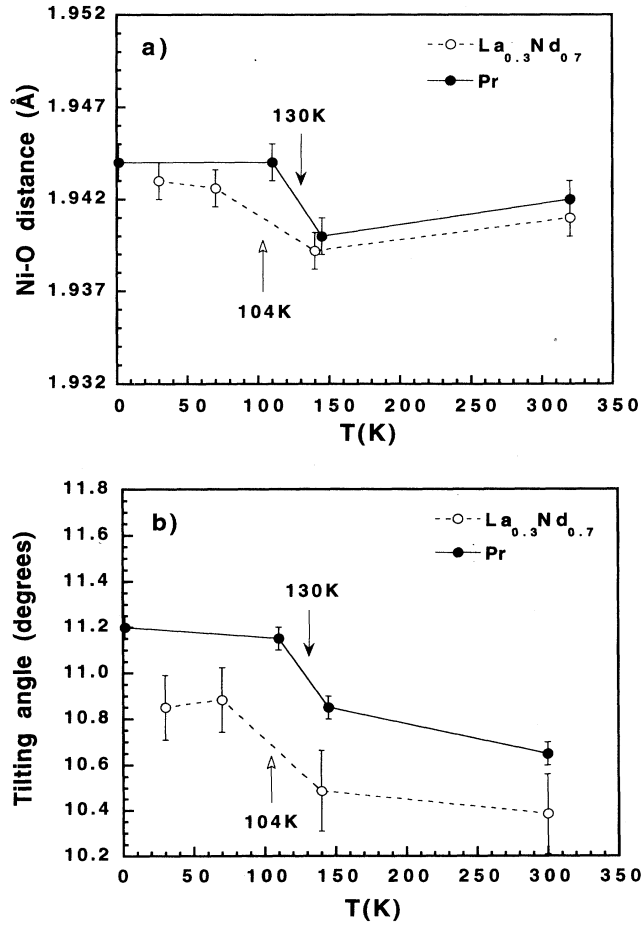

FIG. 6. Average Ni-O distance $d_{\text{Ni-O}}$ and average tilting angle of the NiO_6 octahedra ω for $PrNiO_3$ and $La_{0.3}Nd_{0.7}NiO_3$ at different temperatures and ambient pressure. The dotted lines are guides for the eye.

displayed in Fig. 7. θ, which is the average Ni-O-Ni superexchange angle, has been chosen instead of ω for the sake of clarity. As $\xi(d_{\text{Ni-O}})>0$ and $\xi(\theta)<0$, the difference between these parameters can be better appreciated on the two sides of the $\xi(\alpha)=0$ line. Note that, for the internal pressure, $\zeta(\theta)$ is about 6 times larger than $\zeta(d_{\text{Ni-O}})$ throughout the temperature range studied. In the case of the external pressure, this factor is less than 2, although it is also approximately constant from 1.5 K to RT.

Another important difference between the internal and the external pressure is the temperature dependence of $\zeta(\alpha)$. In the first case, $\zeta(\theta)$ and $\zeta(d_{\text{Ni-O}})$ are practically temperature independent, whereas in the second case their absolute values decrease with T. The modification of the structure under external pressure is then slowed at

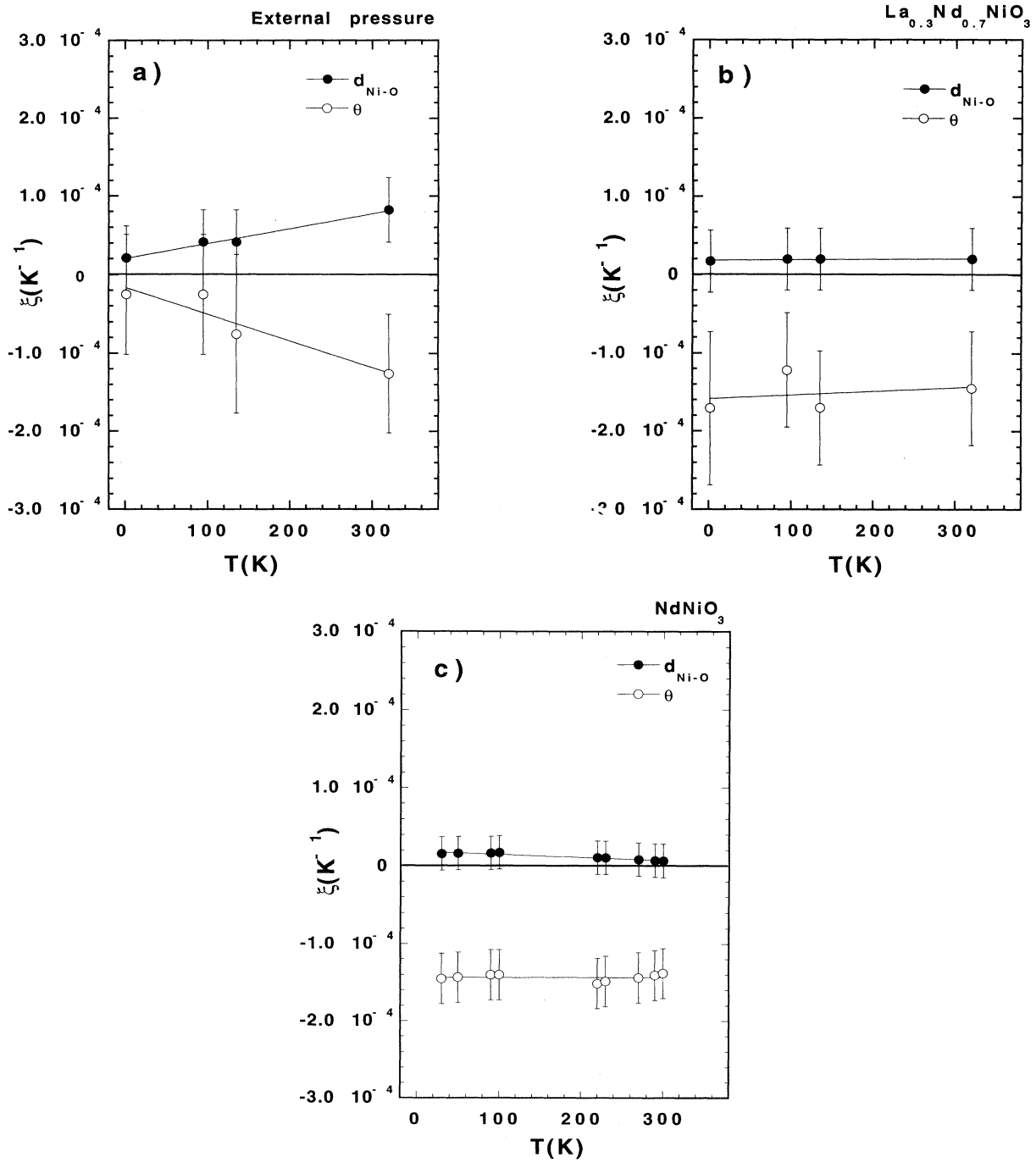

FIG. 7. $\xi(d_{\text{Ni-O}})$ and $\xi(\theta)$ for $PrNiO_3$ under external and internal pressure at different temperatures. The dotted lines are guides for the eye.

low temperatures. This result is not surprising and can be understood as follows: at high temperature, the packing of the ions is not perfect because of thermal agitation. An external pressure will then tend to pack the structure better. At low temperature, a compact packing has already been reached, thus rendering much more difficult the displacement of the ions from their positions. In the case of the internal pressure, the temperature-independent behavior of $\xi(\alpha)$ just indicates that the Pr-O, La-O, and Nd-O bonds have similar expansion coefficients in the temperature range studied.

The origin of structural differences observed by applying internal and external pressure can not be easily inferred from the data presented in this work. The reason is that, in the case of $La_{0.3}Nd_{0.7}NiO_3$, the local distortions introduced in the crystal by partial cation substitution can mask the purely internal pressure effects we are looking for. To overcome this question, we have calculated $\xi(d_{\text{Ni-O}})$ and $\xi(\theta)$ for $NdNiO_3$, which contains only one type of rare-earth ions. The results, which are displayed in Fig. 7(c), are practically identical to these of Fig. 7(b). The local inhomogeneities seem then to have little influence on the variation of θ and $d_{\text{Ni-O}}$, at least in the case of the solid solution studied in this work.

V. MAGNETIC STUDY

The magnetic origin of the new reflections observed in the neutron powder-diffraction patterns below T_{MI} [see Fig. 2(b) and 2(c)] cannot be established without carrying out a polarization analysis. However, the fact that the propagation vector is the same as in $PrNiO_3$ at ambient pressure[18] strongly suggests that the magnetic structure remains unchanged at 4.7 kbar. A Rietveld refinement with the model proposed by García-Muñoz, Rodríguez-Carvajal, and Lacorre[18] gives additional support to this hypothesis. The observed and calculated patterns at 5 K are shown in Fig. 8. The value of the Ni moment at this temperature is $0.92(6)\mu_B$, as expected for Ni^{3+} low spin,

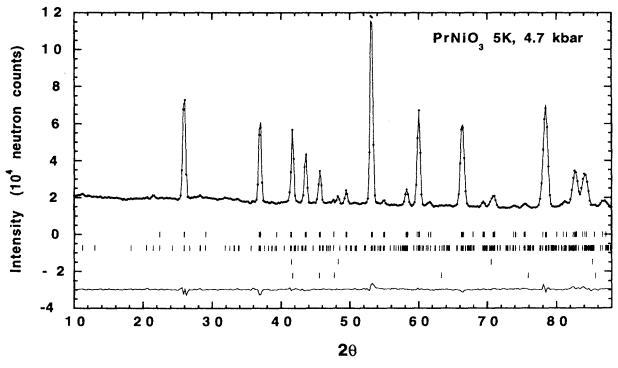

FIG. 8. Observed and calculated HI neutron-diffraction patterns of $PrNiO_3$ at 4.7 kbar and 5 K. The vertical marks show the positions of the allowed reflections. The first row corresponds to nuclear reflections in the *Pbnm* space group; the second row, to the reflections associated to the tridimensional ordering of the Ni magnetic moments; the third to the solid hcp He and the fourth, to the NiO impurity.

and is in complete agreement with the results obtained for $PrNiO_3$ at ambient pressure ($0.93(1)\mu_B$ at 1.5 K).

This result is very difficult to reconcile with the reentrant metallic behavior reported in the resistance measurements under pressure. If below $T_{\text{cr}}=65$ K the sample were metallic, important changes in the ordered Ni magnetic moment, or even its complete disappearance would be expected. However, within the experimental error, its value remains practically constant [$0.92(6)\mu_B$ at 4.7 kbar and 5 K versus $0.93(1)\mu_B$ at ambient pressure and 1.5 K (Ref. 19)]. The increase of the superexchange angle, the decrease of the Ni-O distance and the slightly larger distortion of the NiO_6 octahedron do not seem to affect very much either the spin state of Ni or the magnetic structure.

Another experimental fact supporting the existence of a purely insulating phase below T_{MI} is given by the small evolution of the refined crystallographic parameters. If the samples were metallic between RT and T_{MI}, insulating between T_{MI} and T_{cr} and again metallic below T_{cr}, an increase of the unit-cell volume would be expected across T_{MI} followed by a decrease for $T<T_{\text{cr}}$. As shown in Fig. 4, only the first anomaly can be observed, the value of the volume, the cell parameters, the interatomic distances and angles being approximately the same at both 95 and 5 K.

We believe that the mentioned discrepancies are due to the experimental conditions in which the neutron-diffraction and resistivity measurements were carried out. Concerning the pressure media, note that only in the neutron-diffraction experiments was a purely hydrostatic pressure applied (He gas). In Refs. 3 and 4, two different liquids (1:1 mixture of isoamyl alcohol and *n*-pentane and fluorinert FC-75 (C_6F_{12}), respectively) were used. Thus, even if the pressure is hydrostatic at RT, it is well known that liquids solidify at low temperature and may induce uniaxial stresses in the sample. We then speak of quasihydrostatic pressure, whose effect in the physical properties is not necessarily the same as that of pure hydrostatic pressure. One well-known example is shown by Shelton *et al.*[20] for the A-15 superconducting compounds, where measurements made under hydrostatic and quasihydrostatic pressures may even have different $\partial T_c/\partial P_{\text{ext}}$ signs.

Another parameter crucial for the interpretation of the thermal dependence of the resistance is the cooling/heating rate. In a recent work, Granados *et al.*[5] showed that the resistance displays a strong hysteresis below T_{MI}, the value of R depending on the thermal history of the sample. At high pressures, no systematic studies of this hysteretic behavior have been reported. However, as pointed out by Obradors *et al.*,[4] the decrease of the atomic mobility that takes place by applying an external pressure would probably reduce the transformation rate across the metal-insulator transition. An enhancement of the hysteresis and an increase of the relaxation time necessary to suppress it would be then expected.

In the works of Obradors *et al.*[4] and Canfield *et al.*,[3] the cooling/heating rates were, respectively, 0.2 °/min and 1 °/min. In the neutron-diffraction experiments, the

sample was cooled at 5 K before starting the experiment and maintained at this temperature for two days. The measurements at 95 and 135 K were made by heating the sample, always remaining about two days at the same temperature. Thus, we think that the reentrant metallic behavior observed at low temperature is just the signature of an incomplete relaxation of the system. If the sample is maintained for a sufficiently long time at the same temperature, the insulating behavior is progressively reached, as suggested by the magnetic reflections observed in the low temperature neutron-diffraction patterns.

VI. CONCLUSIONS

The most important conclusion of this work is that the crystallographic structure of $PrNiO_3$ does not react in the same way under application of internal and external pressures. For the same decrease of the metal-insulator temperature, the metallization of the system is accomplished either by a strong decrease of the tilt angle ω (internal pressure) or by moderate diminutions of both ω and $d_{\text{Ni-O}}$ (external pressure). On the other hand, our neutron-diffraction experiments indicate that the magnetic structure observed below $T_N = T_{\text{MI}}$ at ambient pressure is preserved in the pressure range studied. $PrNiO_3$ is then magnetic (and probably insulating) below T_{MI} at 4.7 kbar, in contrast with the results of previous electrical resistance measurements under pressure.

ACKNOWLEDGMENTS

The critical comments of J. Rodríguez-Carvajal and the expert assistance of G. Mélési for operation of the pressure cell are kindly acknowledged. One of the authors (M.M.) thanks also the C.E.E. for financial support under Grant No. ERB4001GT921221.

APPENDIX

For ABX_3 perovskites with *Pbnm* orthorhombic symmetry, it has been shown by O'Keeffe and Hyde[21] that the unit-cell volume can be expressed as

$$V = abc = 32 l^3 \cos^2\phi \ . \tag{A1}$$

Here, a, b, and c are the unit-cell constants in the *Pbnm* setting, l is the B-X bond length, and ϕ is the angle of rotation of the octahedra about the threefold axis. It is important to distinguish ϕ from the tilting angle of the BX_6 octahedra ω (a confusion on this sense was made in Ref. 4). ω is defined as $(\pi-\theta)/2$, θ being the B-X-B superexchange angle. In fact, two different values of θ can be defined for the *Pbmn* symmetry: $\theta_1 = B\text{-}X_1\text{-}B$ and $\theta_2 = B\text{-}X_2\text{-}B$, with X_1 and X_2 being the anions occupying the 2 apical and 4 basal positions of the BX_6 octahedra, respectively. For $RNiO_3$ perovskites (R =Pr,Nd), θ_1 and θ_2 differ only in a few tenths of degree.[9] Thus, in this paper we refer often to its average as $\theta \equiv \langle\theta\rangle = (\theta_1 + 2\theta_2)/2$ and to the average tilting angle as $\omega \equiv \langle\omega\rangle = (\pi - \langle\theta\rangle)/2$. A schematic representation of the *Pbmn* perovskite structure showing the angles ϕ, θ_1, θ_2, ω_1, and ω_2 is displayed in Fig. 9.

An equivalent expression of V as a function of the A-$X(L)$ and B-$X(l)$ bond lengths for A and B in *octahedral* coordination has been given by Reid and Ringwood:[22]

$$V = A L^x l^{3-x} \ . \tag{A2}$$

Here, A and x are two constants that can be determined if V, L, and l are known for some members of a perovskite family. Note that l is exactly the same as in formula (A1). Equating the values of V in (A1) and (A2) we obtain

$$\cos\phi = \left[\frac{A}{32}\right]^{1/2} \left[\frac{L}{l}\right]^{x/2} \tag{A3}$$

and, deriving with respect to the external pressure P_{ext}

$$\left[\frac{\partial \cos\phi}{\partial P_{\text{ext}}}\right]_T = \frac{x}{2}\cos\phi(\kappa_l - \kappa_L) \ , \tag{A4}$$

where κ_l and κ_L are the compressibilities of the B-X and A-X bonds when A and B are in octahedral coordination. The connection between (A4) and the equivalent expressions for ω_1 and ω_2 is given by

$$\cos\omega_1 = \sqrt{3\cos^2\phi/(2+\cos^2\phi)}$$

and

$$\cos\omega_2 = \sqrt{(l+2\cos^2\phi)/3} \tag{A5}$$

which can be easily derived from O'Keeffe's relations[21] (note that we use the setting *Pbnm*),

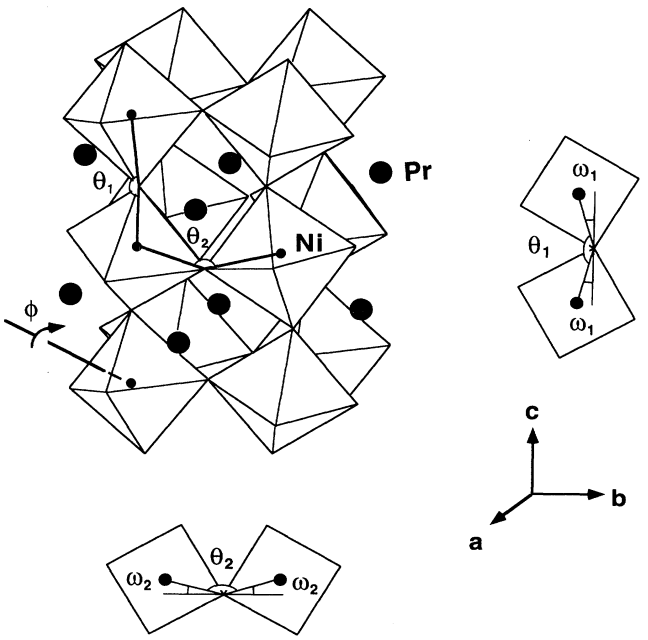

FIG. 9. Schematic representation of the distorted *Pbnm* perovskite structure showing the ϕ, θ_1, θ_2, ω_1, and ω_2 angles.

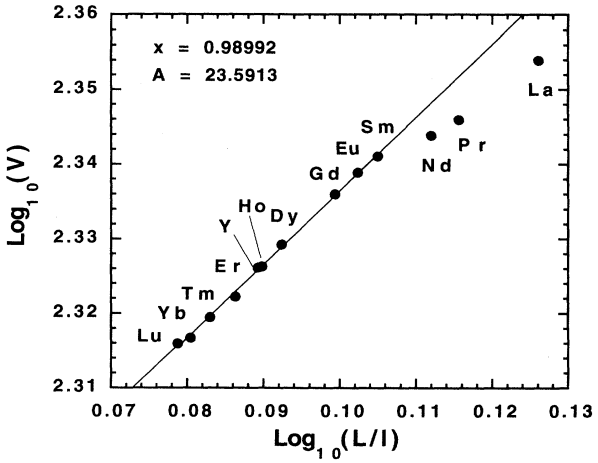

FIG. 10. $\mathrm{Log}_{10}(V)$ versus $\log_{10}(L/l)$ plot for $R\mathrm{NiO}_3$ perovskites. The linear fit includes all the rare earths excepting R=La, Pr, and Nd.

$$b=l\sqrt{[8(2+\cos^2\phi)]/3}=\sqrt{16l^2\cos^2\omega_2-8l^2\cos^2\phi}\ , \tag{A6}$$

$$c=l\sqrt{48/(l+2\sec^2\phi)}=4l\cos\omega_1\ . \tag{A7}$$

Deriving (A4) with respect to P_{ext}, we finally obtain

$$\left[\frac{\partial\cos\omega_1}{\partial P_{\mathrm{ext}}}\right]_T=\frac{x}{2}\left[\cos\omega_1-\frac{1}{3}\cos^3\omega_1\right](\kappa_l-\kappa_L)\ , \tag{A8}$$

$$\left[\frac{\partial\cos\omega_2}{\partial P_{\mathrm{ext}}}\right]_T=\frac{x}{2}\left[\cos\omega_2-\frac{1}{3\cos\omega_2}\right](\kappa_l-\kappa_L)\ , \tag{A9}$$

which are the expressions used in Sec. IV A. Note that in Ref. 4, Eq. (A4) was employed in the place of Eqs. (A8) and (A9).

As was pointed out at the beginning of the Appendix, x (and A) can be determined from the values of V, L, and l. By taking logarithms on the two sides of expression (A2), we have

$$\log_{10}(V)=\log_{10}(Al^3)+x\log_{10}(L/l) \tag{A10}$$

Since the cell parameters,[23] L,[24] and l (1.942 Å) are known for most of the $R\mathrm{NiO}_3$ perovskites, we can plot $\log(V)$ versus $\log(L/l)$. The result is displayed in Fig. 10. A linear least-squares fit gives $x=0.82708$ and $A=24.38105$($R=0.99168$), very close to the values given by O'Keeffe[25] for the perovskites $A^{2+}B^{4+}\mathrm{O}_3$ ($x=0.854$, $A=24.97$).

It is interesting to note that, by excluding from the fit the points corresponding to La, Pr, and Nd, the value of x becomes very close to 1 ($x=0.98992$, $A=23.59133$, $R=0.99912$). If we also exclude the point representative from Lu, we obtain $x=1.0022\approx 1$. It means that, to a very good approximation, V is proportional to L.

The deviations from an $x=1$ law observed for the perovskites with R=La, Pr, and Nd have different origins. In the case of LaNiO_3, they are probably due to the rhombohedral symmetry displayed by this compound (all the remaining nickelates are orthorhombic). For PrNiO_3 and NdNiO_3, we think however that the reason is their anomalous a-b inversion ($b<a<c$ for R=Pr and Nd whereas $a<b<c$ for the remaining rare earths). The meaning of the $V\propto L$ relation for the nickelates with R=Sm, Eu, Gd, Dy, Ho, Y, Er, Tm, Yb, and Lu is however still unclear.

[1]P. Lacorre, J. B. Torrance, J. Pannetier, A. I. Nazzal, P. W. Wang, and T. C. Huang, J. Solid State Chem. **91**, 225 (1991).
[2]M. Medarde *et al.* (unpublished).
[3]P. C. Canfield, J. D. Thompson, S. W. Cheong, and L. W. Rupp, Phys. Rev. B **47**, 12 357 (1993).
[4]X. Obradors, L. M. Paulius, M. B. Maple, J. B. Torrance, A. I. Nazzal, J. Fontcuberta, and X. Granados, Phys. Rev. B **47**, 12 353 (1993).
[5]X. Granados, J. Fontcuberta, X. Obradors, and J. B. Torrance, Phys. Rev. B **46**, 15 683 (1992).
[6]J. Schefer, P. Fischer, H. Heer, A. Isacson, M. Koch, and R. Thut, Nucl. Instrum. Methods Phys. Res. Sect. A **228**, 477 (1990).
[7]J. Rodríguez-Carvajal, Physica B **192**, 55 (1993).
[8]G. Caglioti, A. Paoletti, and F. P. Ricci, Nucl. Instrum. **3**, 223 (1958).
[9]J. L. García-Muñoz, J. Rodríguez-Carvajal, P. Lacorre, and J. B. Torrance, Phys. Rev. B **46**, 4414 (1992).
[10]N. A. Halasa, G. DePasqual, and H. G. Drickamer, Phys. Rev. B **10**, 154 (1974). In this reference, the decrease of ω has been inferred from the evolution of the isomer shifts observed in the high-pressure Mössbauer measurements. To our knowledge, no diffraction data under pressure are available for $R\mathrm{FeO}_3$ compounds.
[11]A. Katrusiak and A. Ratuszna, Solid State Commun. **84**, 435 (1992).
[12]H. K. Mao, R. J. Hemley, Y. Fei, J. F. Shu, L. C. Chen, A. P. Jephcoat, and Y. Wu, J. Geophys. Res. **96**, 8069 (1991). In this reference, only the pressure dependence of the cell parameters of the $\mathrm{Fe}_{1-x}\mathrm{Mg}_x\mathrm{SiO}_3$ series has been measured. The decrease of ω has been inferred from the larger distortion o the unit cell from the ideal cubic structure observed by increasing pressure.
[13]R. M. Hazen and C. T. Prewitt, Am. Mineral **62**, 390 (1977).
[14]J. B. Torrance, P. Lacorre, C. Asavaroengchai, and R. Metzger, J. Solid State Chem. **90**, 168 (1991).
[15]W. A. Harrison, *The Electronic Structure and Properties of Solids* (Freeman, San Francisco, 1980).
[16]R. D. Shannon, Acta Crystallogr. A **32**, 751 (1976).
[17]M. Medarde, J. L. García-Muñoz, S. Rosenkranz, X. Granados, J. Fontcuberta, and P. Lacorre, Physica B **194-196**, 367 (1994).
[18]J. L. García-Muñoz, J. Rodríguez-Carvajal, and P. Lacorre, Phys. Rev. B **50**, 978 (1994).
[19]J. L. García-Muñoz, J. Rodríguez-Carvajal, and P. Lacorre, Europhys. Lett. **20**, 241 (1992).
[20]R. N. Shelton, A. R. Modenbaugh, P. D. Dernier, and B. T. Matthias, Mater. Res. Bull. **10**, 1111 (1975).
[21]M. O'Keeffe and B. G. Hyde, Acta Crystallogr. B **33**, 3802 (1977).

[22]A. F. Reid and A. E. Ringwood, J. Geophys. Res. **80**, 3363 (1975).
[23]G. Demazeau, A. Marbeuf, M. Pouchard, and P. Hagenmuller, J. Solid State Chem. **3**, 582 (1971).
[24]P. Poix, C. R. Acad. Sci. **270**, 1852 (1970).
[25]M. O'Keeffe, B. G. Hyde, and J.-O. Bovin, Phys. Chem. Miner. **4**, 299 (1979).
[26]D. B. McWhan and T. M. Rice, Phys. Rev. Lett. **22**, 887 (1969).
[27]P. C. Canfield, J. D. Thompson, and G. Gruner, Phys. Rev. B **41**, 4850 (1990).
[28]C. N. Berglund and A. Jayoraman, Phys. Rev. **185**, 1034 (1969).
[29]D. B. McWhan, M. Marezio, J. P. Remeika, and P. D. Dernier, Phys. Rev. B **5**, 2552 (1972).